Sci

MDPI

Article

Conventional Platinum Metal Implants Provoke Restenosis Responses in Atherogenic but Not Healthy Arteries

Lea M. Morath [1], Roger J. Guillory II [1], Alexander A. Oliver [2], Shu Q. Liu [3], Martin L. Bocks [4], Galit Katarivas Levy [5], Jaroslaw W. Drelich [6] and Jeremy Goldman [1,*]

1 Department of Biomedical Engineering, Michigan Technological University, Houghton, MI 49931, USA; lmmorath@mtu.edu (L.M.M.)
2 Department of Biomedical Engineering and Physiology, Mayo Clinic Graduate School of Biomedical Sciences, Rochester, MN 55902, USA
3 Department of Biomedical Engineering, Northwestern University, Evanston, IL 60208, USA
4 School of Medicine, UH Rainbow Babies & Children's Hospital, Case Western Reserve University, Cleveland, OH 44106, USA
5 Department of Biomedical Engineering, Ben Gurion University, Beersheba 8400711, Israel
6 Department of Materials Science and Engineering, Michigan Technological University, Houghton, MI 49931, USA
* Correspondence: jgoldman@mtu.edu; Tel.: +1-(906)-487-2851

Abstract: Platinum-containing stents are commonly used in humans with hypercholesterolemia, whereas preclinical stent evaluation has commonly been performed in healthy animal models, providing inadequate information about stent performance under hypercholesterolemic conditions. In this investigation, we used an ApoE$^{-/-}$ mouse model to test the impact of hypercholesterolemia on neointima formation on platinum-containing implants. We implanted 125 µm diameter platinum wires into the abdominal aortas of ApoE$^{-/-}$ and ApoE$^{+/+}$ mice for 6 months, followed by histological and immunofluorescence examination of neointimal size and composition. It was found that ApoE$^{-/-}$ mice developed neointimas with four times larger area and ten times greater thickness than ApoE$^{+/+}$ counterparts. Neointimas developed in the ApoE$^{-/-}$ mice also contained higher amounts of lipids quantified as having 370 times more coverage compared to ApoE$^{+/+}$, a 3-fold increase in SMCs, and a 22-fold increase in macrophages. A confluent endothelium had regenerated in both mouse strains. The ApoE$^{-/-}$ mice experienced luminal reductions more closely resembling clinically relevant restenosis in humans. Overall, the response to platinum arterial implants was highly dependent upon the atherogenic environment.

Keywords: ApoE knockout; platinum; biocompatibility; stent material

check for updates

Citation: Morath, L.M.; Guillory, R.J., II; Oliver, A.A.; Liu, S.Q.; Bocks, M.L.; Levy, G.K.; Drelich, J.W.; Goldman, J. Conventional Platinum Metal Implants Provoke Restenosis Responses in Atherogenic but Not Healthy Arteries. *Sci* **2023**, *5*, 25. https://doi.org/10.3390/sci5020025

Academic Editor: Anastasios Lymperopoulos

Received: 15 May 2023
Revised: 5 June 2023
Accepted: 9 June 2023
Published: 19 June 2023

Copyright: © 2023 by the authors. Licensee MDPI, Basel, Switzerland. This article is an open access article distributed under the terms and conditions of the Creative Commons Attribution (CC BY) license (https://creativecommons.org/licenses/by/4.0/).

1. Introduction

The first successful bare-metal coronary stents were made from stainless steel in the 1980s and gained FDA approval in the 1990s. However, due to a 10–30% occurrence of in-stent restenosis [1], drug-eluting stents (DES) were developed with polymer coatings over the stainless steel. The DES reduced restenosis rates, but experienced higher occurrences of late-stage thrombosis [2]. Platinum was first studied as the main constituent of bare-metal stent materials in the 1990s and early 2000s, experiencing a 30–70% reduction in lumen diameter in pig models [2,3]. This resulted in the alloying of platinum to improve the restenosis rates, such as in platinum–chromium materials currently used for clinical applications. However, platinum has still been used as a reference material in the development of biodegradable implant metals [4,5].

Unfortunately, because all stent materials go through biocompatibility evaluation in healthy animal arteries, many bio*in*compatibility problems go undetected until widespread use of the device in humans [6]. In our view, the reliance upon healthy animal models

has hindered materials development and human treatment. Materials development for stents could be substantially improved by testing in animal models that more closely reflect the diseased arterial environment, such as the widely used apolipoprotein E (ApoE) knockout mice.

A transgenic mouse lacking the gene for ApoE was introduced by Nobuyo Maeda in 1992 [7] and has been widely used by molecular biologists over the past three decades. The ApoE protein attaches to remnant very-low-density lipoproteins (VLDLs) and chylomicrons to signal for their removal from arteries for recycling or excretion as waste by the liver. Mice lacking the ApoE protein form atherosclerotic plaques around 3–4 months that are similar to those seen in humans [8]. Although this animal model of arterial disease has been most commonly used to investigate the molecular mechanisms of atherosclerosis, it has also been used on occasion to test the efficacy of arterial devices in a diseased environment. Matter et al. and Ali et al. found that ApoE knockout ($ApoE^{-/-}$) mice had larger neointimas and increased cell proliferation after balloon angioplasty when compared to wild-type (WT) mice [9,10]. Additionally, Ali et al. found that neointimas were 30% larger in $ApoE^{-/-}$ relative to WT mice 28 days after balloon angioplasty and were an additional 30% larger than WT mice after stenting [9]. Surprisingly, aside from these few works focused on evaluating the efficacy of arterial devices, the $ApoE^{-/-}$ mouse has not been used to develop and optimize biomaterials intended for constructing vascular devices. The relative lack of biocompatibility studies in the $ApoE^{-/-}$ mouse may be due to major technical challenges when using mice for the development of devices intended for humans, namely the considerable micro-vascular surgical skill and lack of delivery devices required to introduce human-intended devices into small mouse anatomy. Technical difficulty coupled with a lack of FDA requirements to evaluate materials or devices in disease models has discouraged material development using small animal models of arterial disease. Indeed, the primary use of the $ApoE^{-/-}$ mouse has been to investigate non-surgical therapies for coronary artery disease (CAD), including anti-inflammatory agents [11] and diet modifications [12,13].

Fortunately, candidate materials for arterial devices can be evaluated in early exploratory work using simplified geometries. Our group was the first to introduce a wire implantation approach for rats in 2012 [14]. In this approach, a wire with a diameter of ~0.25 mm is surgically implanted into the abdominal aorta of Sprague–Dawley rats [15]. We have used this approach to investigate the in vivo corrosion behavior and biocompatibility of a wide range of zinc alloys [16]. Others have investigated wires made of stainless steel and magnesium alloys [17]. The primary advantage of a wire implantation/murine model vs. a stent/large animal model is that the lower cost and smaller animals can be leveraged to increase sample sizes for comprehensive investigations of the biological response to many novel materials. Other advantages include simplified materials preparation and reduced surgical skill and instrumentation requirements. The wire implantation approach also removes the variable of injury from balloon and stent expansion.

Here, we have adapted our well-established arterial wire-implant approach [14] to bridge the fields of molecular biology and materials science by investigating the biocompatibility of a conventional arterial device material in the aortas of atherogenic $ApoE^{-/-}$ transgenic mice. This approach allows for the evaluation of stent materials with a high sample size in a realistic animal model of human arterial disease. In the present study, platinum was selected as the implantation material to demonstrate the difference in biological response in healthy vs. diseased arterial environments. This selection is due to the incorporation of platinum into medical devices in clinical use [18,19] and the previous use of platinum wires in a number of studies as a reference material for novel biodegradable implant metals [4,5]. The present work paves the way for materials scientists to access major advances in the development of small animal models of human arterial disease that have never before been adapted to benefit the development of arterial device materials.

2. Materials and Methods

2.1. Implantation

Platinum wires (99.95% purity, PT00-WR-000117, Goodfellow, Inc., Huntingdon, UK) of 125 µm diameter were implanted into female 10-week-old ApoE$^{-/-}$ and ApoE$^{+/+}$ mice (n = 9 for each mouse type) using a procedure similar to that previously published for rats [15]. All mice had a C57BL/6 genetic background and were fed a normal chow diet for the duration of the study. Eight aortas were collected from age-matched ApoE$^{-/-}$ mice without operation or implantations. All animal experiments were approved by the Michigan Technological University Institutional Animal Care and Use Committee (IACUC) board. The overall experimental scheme is shown in Figure 1.

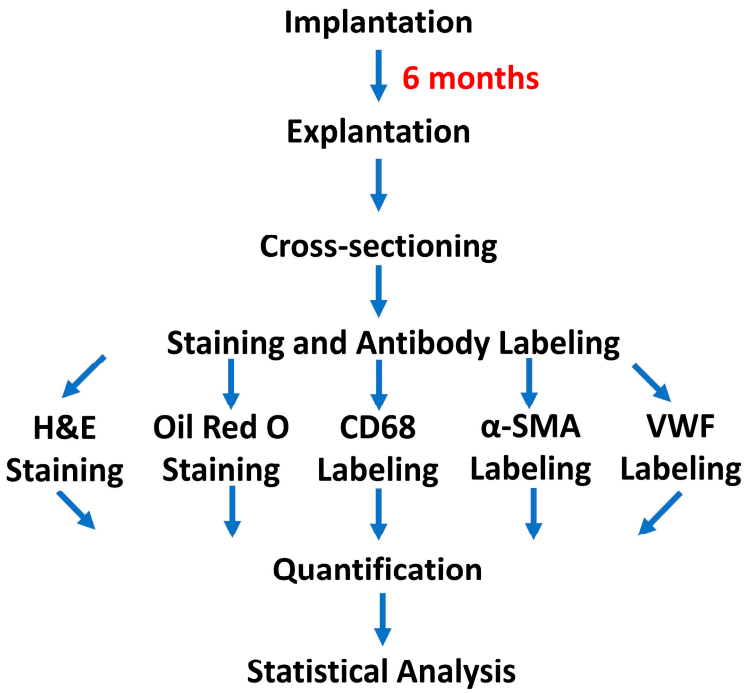

Figure 1. Experimental scheme.

2.2. Implant Removal

After 6 months, the animals were euthanized, and the implants were removed according to previously published protocols [15]. Each wire was placed in a small cryo-mold with optimal cutting temperature medium (OCT) (Thermo Fisher Scientific, Waltham, MA, USA) and flash-frozen using liquid nitrogen. The samples were then stored at −80 °C until cryo-sectioning.

2.3. Cryo-Sectioning

Samples were cryo-sectioned using an HM525 NX Thermo Fisher Scientific cryo-microtome. Each sample was attached to a specimen chuck using OCT. The sample was orientated to ensure a cross-sectional cutting direction. Each sample was cryo-sectioned at −25 °C with a thickness of 9 µm. The sample was rapidly cryo-sectioned without collection of sections until the wire could be seen to have progressed past the internal elastic lamina by visual inspection. Then, the sample was carefully sectioned and sections were collected on Histobond slides (VWR, Radnor, PA, USA). The sample was sectioned while the wire was located in the artery lumen adjacent to the intima, mimicking a single stent strut. All slides were stored at −80 °C for later staining.

2.4. Staining

2.4.1. Reagents

For hematoxylin and eosin (H&E) staining, the reagents included 10% neutral buffered formalin and phosphate-buffered saline (PBS), obtained from Thermo Fisher Scientific, and Gill's Hematoxylin No. 3, 1M hydrochloric acid, 100% ethanol, Eosin Y disodium salt, acetic acid 99.7%, xylene substitute, and Eukitt® quick hardening mounting medium, all of which were obtained from Sigma-Aldrich (Burlington, MA, USA).

For Oil Red O staining, the reagents included 10% neutral buffered formalin, PBS, deionized water (DI water), isopropanol, and Oil Red O solution 0.5% in isopropanol obtained from Sigma-Aldrich, along with Gill's hematoxylin No. 3, 1M hydrochloric acid, and aqueous mounting media.

For immunofluorescence staining, the reagents included absolute ethanol, methanol, paraformaldehyde from Thermo Fisher Scientific, PBS and goat serum from Sigma-Aldrich, and endogenous avidin and biotin blocks obtained from Abcam. The primary antibodies were anti-CD68 (ab125212), anti-alpha smooth muscle Actin (ab5694), and anti-VWF (GTX74137). The secondary antibody used for CD68 was biotinylated goat anti-rabbit IgG (ab6720). Streptavidin Alexa flour 488 conjugate (S11223) obtained from Thermo Fisher Scientific and goat antirabbit IgG Alexa fluor 488 (ab150077) and donkey anti-sheep IgG (ab175712) obtained from Abcam contained the fluorescent molecules. All specimens were also stained with 4′,6-diamidino-2-phenylindole (DAPI). Aqueous mounting medium (Thermo Fisher Scientific) was used to mount coverslips.

2.4.2. H&E Staining

H&E staining was performed to allow for qualitative analysis of vessel morphology and cell types. For H&E staining, cross-sections were fixed in 10% neutral buffered formalin for 15 min. The slides were then washed in three changes of PBS and one wash of deionized water, each for 5 min, to remove any excess formalin. The samples were placed in Gill's Hematoxylin No. 3 for 5 min and differentiated in a regressive solution with a pH of 1.8–2.0. The slides were then "blued" in tap water for 5 min and washed two times in 95% ethanol for 5 min each. An Eosin Y working solution was used to counterstain the samples for 30 s and differentiated in 95% ethanol. The stain was checked under a microscope with 10× magnification. Afterward, the slides were dehydrated in two changes of 100% Ethanol for 5 min each. Next, the slides were optically cleared using two changes of xylene substitute, 5 min each, and finally mounted under a coverslip using Eukitt quick hardening mounting medium. The slides were imaged at a magnification of 40× on a Zeiss Axioscan.

2.4.3. Oil Red O Staining

Oil Red O staining was utilized to evaluate lipid presence in the neointima. Slides were fixed in 10% neutral buffered formalin for 15 min, followed by three PBS washes and a DI water wash for 5 min each. Then, the cross-sections were placed in a 60% isopropanol wash for 5 min. The slides were stained in a 60% Oil Red O stain solution for 10 min and differentiated in 60% isopropanol. Next, the sections were rinsed with DI water for 5 min before being counterstained with Gill's hematoxylin No. 3. After regression of the counterstain, coverslips were mounted using an aqueous mounting media.

2.4.4. Alpha-Smooth Muscle Actin Staining

Alpha-smooth muscle actin staining was performed to determine the extent of smooth muscle cell presence in the neointimal tissue. The specimens were fixed in ice-cold methanol for 5 min and quickly washed three times in PBS before 10% goat serum was applied for 30 min. The primary antibody was used with a dilution of 1:500 (v/v) in PBS for an incubation time of 1 h. The secondary antibody was diluted 1:300 (v/v) in PBS and remained on the specimens for an hour. DAPI was applied with a dilution of 1:1000 (v/v) for 2 min and then coverslips were placed using aqueous mounting medium. The slides were imaged using the appropriate fluorescent filters at 40× magnification.

2.4.5. CD68 Immunofluorescence Staining

CD68 immunofluorescence labeling was performed to assess macrophage presence and distribution. The slides were fixed in pure ethanol for 2 min and then washed three times with PBS for 5 min each wash. The slides were treated with 10% (v/v) goat serum diluted in PBS for 30 min and then endogenous biotin and avidin blocks for 10 min each. The primary antibody was diluted 1:100 (v/v); the secondary antibody and streptavidin antibody were diluted 1:500 (v/v). All antibody dilutions were in PBS and solutions were left on the specimens for 1 h. DAPI was diluted 1:1000 (v/v) and placed on slides for 2 min. Then, coverslips were applied using aqueous mounting medium. Slides were washed twice using PBS between each step. The slides were imaged at a magnification of 40× using a Zeiss Axioscan.

2.4.6. Von Willebrand Factor (VWF) Immunofluorescence Staining

VWF immunofluorescence labeling was performed to examine the confluence of the endothelial layer of the artery. The slides were fixed in paraformaldehyde for 10 min and then washed three times in PBS before being treated with 10% (v/v) donkey serum for 30 min. The primary antibody was diluted 1:2000 (v/v) and the secondary was diluted 1:1000 (v/v). Both antibodies were diluted in PBS and placed on the slides for 1 h each. Then, the slides were labeled with DAPI for 2 min with a dilution of 1:1000 (v/v) and coverslipped. The slides were imaged at a magnification of 40× using a Zeiss Axioscan.

2.5. Quantification

H&E images were used to quantify the wire-to-lumen thickness (WLT) and neointimal area (NA) as previously described [15]. Oil Red O images were thresholded in grayscale to determine the lipid concentration within the neointima. CD68, α-SMA, and VWF images were thresholded to determine the coverage of the fluorescent signal and therefore the coverage of macrophages and smooth muscle cells within the neointima and the confluence of endothelial lining, respectively.

2.6. Statistics

All statistical analyses were performed using MATLAB R2017a. A Shapiro–Wilk test was used to test the normality of each dataset. Datasets with a p-value less than 0.05 were considered to have a non-normal distribution. Morphometric, CD68, and Oil Red O data were considered to be normal without transformation. α-SMA data were considered to have a non-normal distribution and were subsequently transformed using the square root function prior to statistical analysis. A Welch's t-test was performed to find differences between the mean of ApoE$^{-/-}$ and ApoE$^{+/+}$ mice for each dataset, with a p-value < 0.05 as the threshold for determining statistical significance.

3. Results

3.1. Morphometric Analysis

H&E staining was performed to inspect the general morphological features of the neointimal response to the implant. Measurements of the images were conducted for morphometric analysis of wire-to-lumen thickness (WLT) and neointimal area (NA) of neointimas that formed around the platinum implants in both mouse groups, and also including NA measurements for non-implanted age-matched control ApoE$^{-/-}$ mice. Figure 2A,B shows representative images of the arterial response to platinum in ApoE$^{-/-}$ and ApoE$^{+/+}$ mice. As shown in Figure 2A, ApoE$^{-/-}$ mice developed heavily cellularized areas around the implant and within the neointimal cap. In between these regions is an area of largely acellularized tissue with large gaps in the extracellular matrix. In contrast, ApoE$^{+/+}$ mice developed uniformly distributed cells throughout the neointima, as shown in Figure 2B. The nuclei in ApoE$^{+/+}$ mice have a lower density than the nuclei in ApoE$^{-/-}$ mice, which may reflect an increased infiltration of inflammatory cells in the ApoE$^{-/-}$ mice. In contrast to ApoE$^{-/-}$ mice with implants, which all experienced substantial neointimal development,

6 out of 8 non-implanted ApoE$^{-/-}$ mouse arteries experienced only mild to moderate neointimal development due to the diseased background condition (Figure 2E). In general, neointimal growth of the ApoE$^{-/-}$ mice tended to be more severe at the curved and branched regions of the arterial system, whereas a straight portion of the abdominal aorta was selected for implantation. Therefore, the more severe neointimal growth seen in the implanted mice was due primarily to a biological response to the material. Figure 2F,G shows the difference between groups for WLT and NA metrics in graphical form. The ApoE$^{-/-}$ mice developed neointimal tissue with a thickness of about 150 µm and an area of about 0.20 mm^2 from the implant into the arterial lumen that is nearly ten times thicker and four times larger than neointimal tissue in the ApoE$^{+/+}$ mice. The NA for the age-matched control condition was not statistically different from the other two groups. These results demonstrate that the atherogenic ApoE$^{-/-}$ mice experience a more severe neointimal response to a conventional metal implant relative to healthy counterparts.

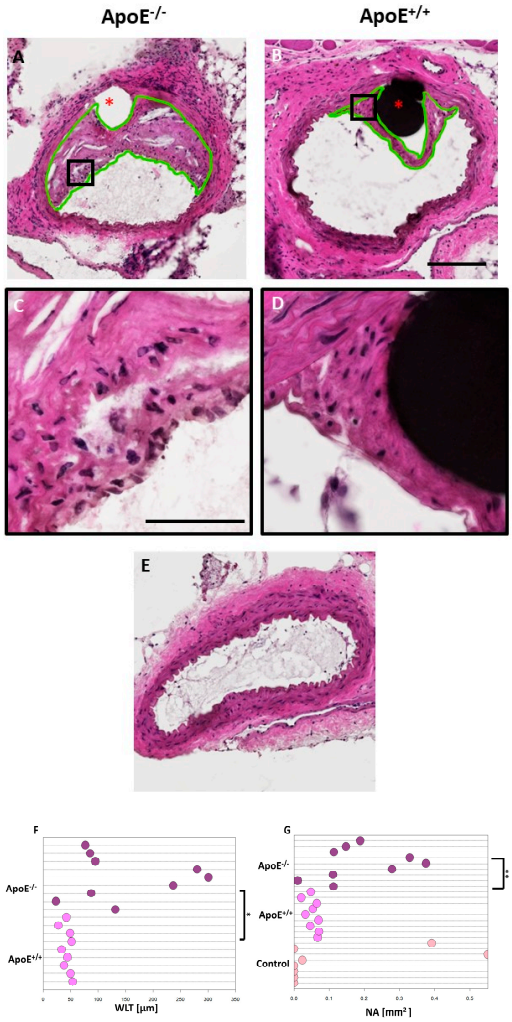

Figure 2. (**A**,**B**) Representative H&E images for ApoE$^{-/-}$ and ApoE$^{+/+}$ groups, respectively. Red asterisk identifies the implant site. The green line outlines the neointima. Black box identifies area selected for high magnification. (**C**,**D**) High-magnification H&E images for ApoE$^{-/-}$ and ApoE$^{+/+}$ groups, respectively. (**E**) Typical non-implanted, age-matched ApoE$^{-/-}$ control artery showing mild neointimal thickening at some locations. (**F**) Average WLT with standard error for each group. * represents statistical significance (p-value = 0.015, n = 9). (**G**) Average NA with standard error for each group. ** represents statistical significance (p-value = 0.010, n = 9) based on Welch's t-test. Scale bar in (**B**) is 200 µm. Scale bar in (**C**) is 50 µm.

3.2. Lipid Staining

Oil Red O staining was utilized to semi-quantify the amount of lipid deposition in the neointima of both mouse types following platinum implantation. Figure 3 shows representative images for each mouse group and a graphical representation of the average Oil Red O stain determined by thresholding of the images. It was found that ApoE$^{-/-}$ mice experienced a significantly larger amount of lipid deposition, with an average lipid coverage of ~13,400 pixels compared to 36 pixels in ApoE$^{+/+}$ mice ($p = 9.3 \times 10^{-4}$). This finding is in accordance with the well-known atherogenic environment in the ApoE$^{-/-}$ mice. Interestingly, the lipid accumulation is concentrated in the neointimal cap in the ApoE$^{-/-}$ mice. Lipid deposition in the non-implanted ApoE$^{-/-}$ artery shown in Figure 3E is also concentrated within the neointimal growth. Only 2 of 8 age-matched non-implanted arteries showed a severe presence of lipids, which also concentrated within the neointimal tissue. In general, there was a lack of lipid deposition in the ApoE$^{-/-}$ arterial wall, regardless of implant presence. Therefore, it appears that the lipid accumulation preferentially concentrates within the neointimal tissue and specifically within the fibrous cap of the implanted mice.

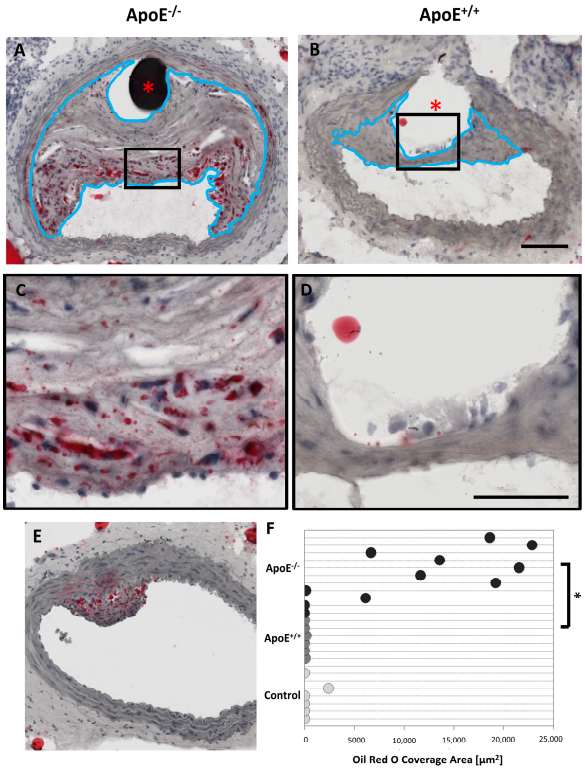

Figure 3. (**A**,**B**) Representative Oil Red O images for each group. Red asterisk identifies the implant site. The blue line outlines the neointima. Black box identifies the area selected for high magnification. (**C**,**D**) High-magnification Oil Red O images for ApoE$^{-/-}$ and ApoE$^{+/+}$ groups, respectively. (**E**) Representative abdominal aorta without implant from age-matched ApoE$^{-/-}$ mouse. (**F**) Average Oil Red O signal with standard error for each mouse group. * represents statistical significance (p-value = 9.3×10^{-4}, $n = 9$). Scale bar in (**B**) is 100 μm. Scale bar in (**D**) is 50 μm.

3.3. α-SMA Immunofluorescence

α-SMA immunofluorescence was employed to quantify the amount of smooth muscle cell presence in the neointima. Figure 4 displays representative images of α-SMA staining for each group and a graphical depiction of the average α-SMA signal. ApoE$^{-/-}$ mice had a 3-fold increase in α-SMA signal (3200 + 744) compared to ApoE$^{+/+}$ mice (1000 + 517) (p-value = 0.0107) with the signal concentrated in the neointimal cap. ApoE$^{+/+}$ mice also displayed a concentration of SMCs within the neointimal cap.

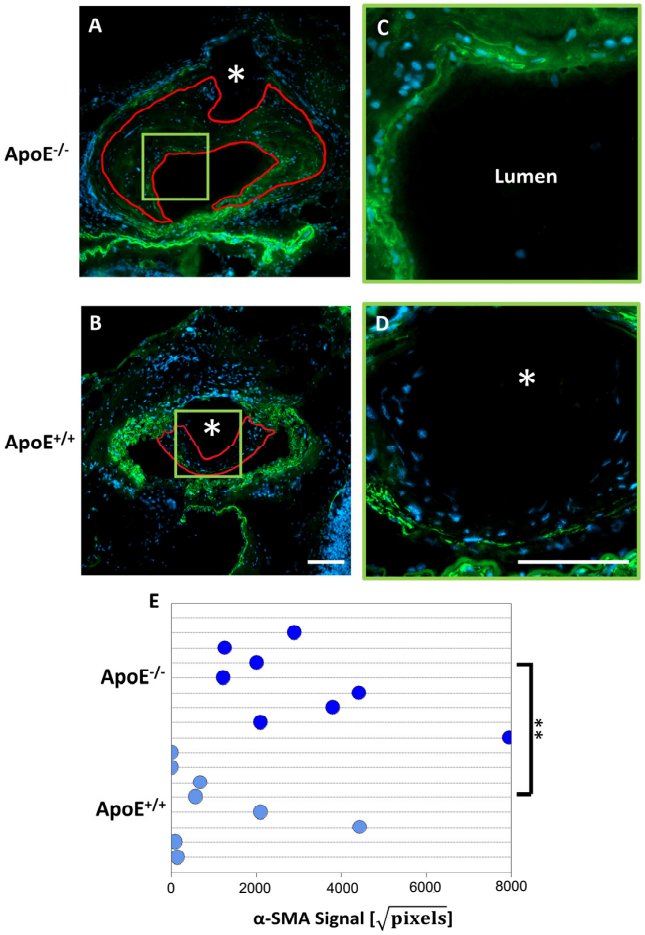

Figure 4. (**A**,**B**) Representative α-SMA images for each group. White asterisk (*) identifies the implant site. The red line outlines the neointima. Green box identifies area of high magnification image. (**C**,**D**) High-magnification α-SMA images for ApoE$^{-/-}$ and ApoE$^{+/+}$ groups, respectively. (**E**) Average α-SMA signal coverage with standard error for each group. ** represents statistical significance (p-value = 0.0107, n = 9). Scale bar in (**B**) is 100 μm. Scale bar in (**D**) is 50 μm. Green: α-SMA. Blue: DAPI-stained cell nuclei.

3.4. CD68 Immunofluorescence

Immunofluorescence labeling was utilized to determine the amount of macrophage infiltration and inflammation due to platinum metal implantation. Figure 5A,B shows representative images for both groups and Figure 4C shows a graphical representation of the average CD68 signal. It was found that the atherogenic ApoE$^{-/-}$ mice experienced a 22-fold increase in the CD68 signal relative to the healthy ApoE$^{+/+}$ counterparts. This indicates that macrophage infiltration is increased due to the presence of the platinum implant in the disease condition of the ApoE$^{-/-}$ mice, an effect that is similar to diseased human arteries [20]. The CD68 signal increases towards the luminal-facing surface of the neointima for the ApoE$^{-/-}$ mice, which corresponds to the region of increased lipid deposition shown in Figure 3. No such inflammation-concentrated region is seen in the ApoE$^{+/+}$ or non-implanted ApoE$^{-/-}$ mice counterparts. Macrophages are well known to form foam cells and worsen plaque formation in their effort to metabolize accumulating arterial lipids. The near complete lack of CD68 signal in the non-implanted ApoE$^{-/-}$ mice and ApoE$^{+/+}$ counterparts suggests that the presence of the metal implant in the context of an atherogenic environment stimulates an intense macrophage response.

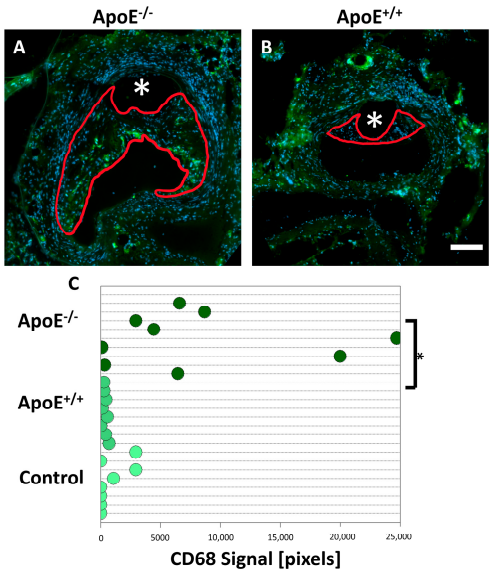

Figure 5. (**A**,**B**) Representative CD68 images for each group. White asterisk identifies the implant site. The red line outlines the neointima. (**C**) Average CD68 signal coverage with standard error for each group. * represents statistical significance (p-value = 0.0244, n = 9). Scale bar in (**B**) is 100 µm. Green: CD68. Blue: DAPI-stained cell nuclei.

3.5. Von Willebrand Factor (VWF) Immunofluorescence

VWF labeling was used to determine the extent of reendothelialization over the neointimal tissue. As shown in Figure 6, the endothelium had returned to confluence in both groups. This suggests that the hyperlipidemia environment, larger neointima, and manifold increase in inflammation in ApoE$^{-/-}$ mice may not hinder endothelium regeneration.

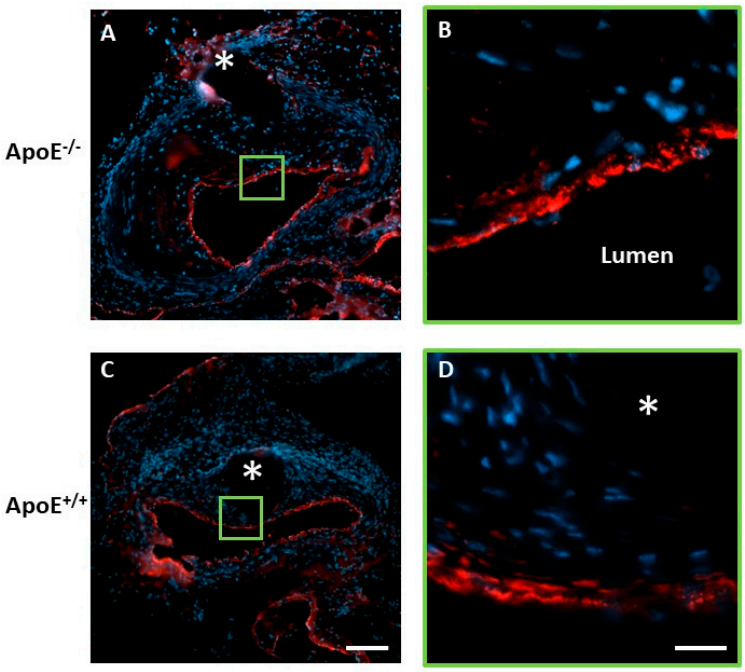

Figure 6. (**A**) Representative VWF labeling for ApoE$^{-/-}$ group. Green box identifies area of high magnification image. White asterisk (*) identifies the implant site. (**B**) Representative high-magnification VWF image for ApoE$^{-/-}$ group. (**C**) Representative VWF labeling for ApoE$^{+/+}$ group. White asterisk identifies the implant site. Green box identifies area of high-magnification image. Blue color is DAPI-labeled cell nuclei. Scale bar is 100 µm. (**D**) Representative high-magnification image for ApoE$^{+/+}$ image. Scale bar is 25 µm.

4. Discussion

Because the evaluation of materials in conventional healthy animal models may conceal many fundamental material performance challenges inherent to the environment of diseased arteries, including heightened inflammation, lipid deposition, and smooth muscle cell activation, we speculated that evaluating material behavior and biocompatibility in the aortas of atherogenic ApoE$^{-/-}$ transgenic mice could provide valuable feedback for materials development.

Although healthy animals are widely used for vascular material biocompatibility evaluations, the arteries of healthy animals do not naturally develop atherosclerosis. Furthermore, most of their cholesterol is transported as high-density lipoproteins (HDLs), whereas most human cholesterols are transported as low-density lipoproteins (LDLs). Several transgenic mouse models have been developed to recapitulate the human atherosclerosis disease condition. These models generally utilize the deletion or disruption of genes that encode cell receptors involved in lipid metabolism. Ldlr$^{-/-}$, for example, knocks out the LDL receptors on cell membranes to reduce the endocytosis of LDLs from the bloodstream. This creates a mouse with higher plasma cholesterol levels of 200–300 mg/dL compared to 75–110 mg/dL in wild-type mice. However, these mice are more prone to diabetes and obesity, making them useful for studying the effects of comorbidities on atherosclerosis [21], but a poor choice for focusing on the effects of atherosclerosis on implant-dependent neointima development. Furthermore, this mouse strain is more resistant to injury from implants, further complicating the study of effects from biometal implants [22]. Other transgenic mice, such as Apoe*3-Leiden.CETP (cholesterol ester transfer protein) and leptin- or leptin receptor-deficient mice can be used to study the effects of other comorbidities such as metabolic syndromes and obesity. We selected ApoE$^{-/-}$ mice to investigate biometal implant biocompatibility because these mice spontaneously develop atherosclerosis on a normal diet and at a young age without the influence of comorbidities, as is the case with other transgenic lines [21]. An ApoE$^{-/-}$ mouse model may be beneficial for developing biointeractive stent materials due to the similarities between the diseased human and the diseased mouse model in terms of the atherogenic environment. Moreover, there is extensive knowledge about the disease mechanisms in these mice, which can contribute to our understanding of biological responses to the biometals.

Analysis of the wire-to-lumen thickness (WLT) and neointimal area (NA) metrics supported the observation that the biological response to platinum was dramatically more aggressive in the ApoE$^{-/-}$ mouse. Significant increases were detected for neointimal size for both metrics, demonstrating a strong neointima projection into the arterial lumen. Importantly, increases in neointimal size reduce the cross-sectional luminal area available for blood circulation. Therefore, materials that provoke a pronounced neointimal area growth are not favored for the treatment of atherosclerosis, where the purpose of implantable devices is to restore blood flow through the vessel. Although platinum is considered a biocompatible metal, our findings suggest that platinum implantation elicits a strong neointimal growth response and inflammation in the context of the lipid-rich environment that is typical of atherosclerotic human arteries. These findings are consistent with those previously reported by Ali et al., who saw a 3-fold increase in neointimal hyperplasia in ApoE$^{-/-}$ mice after balloon angioplasty and stent placement [9].

We also found a 3-fold increase in SMC neointimal content in association with the increased neointimal size. This suggests that SMCs are a major component of the neointima in the ApoE$^{-/-}$ mouse, similar to findings in human subjects [22]. A 22-fold increase in CD68 macrophage labeling was also detected, demonstrating a potent increase in inflammation, consistent with the well-known chronic inflammation present in both ApoE$^{-/-}$ mice and atherosclerotic human arteries [23]. A similar increase in inflammation was found by Matter et al. and Ali et al. after balloon angioplasty and stent placement [9,10]. The pronounced increase in neointimal size may be the result of a strong SMC infiltration and macrophage activation working in tandem, as a positive correlation between macrophages, SMCs, and neointimal size has been found by some research groups [24]. The benign

biological response to platinum in the healthy control mice reinforces the notion that candidate stent materials should be evaluated in disease models, such as the ApoE$^{-/-}$ mouse, to avoid making incorrect predictions regarding the biocompatibility of implant metals in atherogenic arteries based on biocompatibility studies undertaken in healthy arteries. Indeed, inert materials were considered the gold standard for arterial implants in the 1970s, whereas bioactive coatings of these materials were later found to be required to reduce widespread restenosis responses [25].

Bare metal stents implanted in diseased human arteries frequently provoke restenosis and late-stage thrombosis, where clinically relevant restenosis requiring medical intervention is considered as a $\geq$75% reduction in luminal area [24]. It has also been found that the macrophage signal is strongest near stent struts and that SMCs are often the predominant cell type in the neointimal tissue. In some cases, plaque forms within the stent struts at late time points [26]. Similar characteristics are seen in ApoE$^{-/-}$ mice, with an average luminal area reduction of 65 $\pm$ 9% vs. 30 $\pm$ 13% for ApoE$^{+/+}$ at the investigated 6-month time point. Therefore, the response to an inert platinum implant in the ApoE$^{-/-}$ mice more closely reflects the restenosis response to bare metal stents in diseased human arteries as compared to the healthy animal arteries that are routinely used to evaluate and develop vascular materials. This similarity in response between the ApoE$^{-/-}$ mice and humans may be due to the extensive lipid deposition and inflammation seen in the ApoE$^{-/-}$ neointima, verified by Oil Red O staining and CD68 labeling.

Although we believe the ApoE$^{-/-}$ mouse may represent the best transgenic mouse model for evaluating the performance of candidate stent materials in a realistic atherogenic environment, our wire implant approach can be readily applied to investigations of the in vivo biological response using alternative transgenic models. For instance, specific genetic modifications using transgenic technology could be leveraged to provide mechanistic insight into device endothelialization, device thrombosis, and neointimal hyperplasia and inflammation around biometal implants. Just as importantly, the approach introduced in the present contribution can be easily adapted to investigate the effects of different bulk material compositions, including those of biodegradable metals, various bulk treatments and coatings, and even drug elution, simply by implanting wires made with biodegradable compositions and experimental coatings into arteries of the transgenic ApoE$^{-/-}$ mouse.

A limitation of the ApoE$^{-/-}$ mouse model is that atherosclerotic lesions rarely progress to advanced stages with atherothrombotic vascular occlusion, as observed in humans. ApoE-deficient mice fed a high-fat diet and infused with angiotensin II for 4 weeks might represent a more valuable model for studying the biocompatibility of arterial device materials as this treatment accelerates the destabilization and vulnerability of the plaques to rupture.

5. Conclusions

When compared with ApoE$^{+/+}$, ApoE$^{-/-}$ mice implanted with platinum displayed:

1. Larger neointimal tissue growth in terms of WLT and NA;
2. A 22-fold increase in macrophage coverage;
3. A 3-fold increase in SMC presence;
4. A 370-fold increase in lipid deposition.

These results demonstrate the importance of selecting an appropriate biological environment within which to evaluate the biocompatibility of vascular implant materials. This is particularly important for metals that are commonly implanted into diseased environments.

Author Contributions: Conceptualization, J.G. and J.W.D.; methodology, J.G.; software, L.M.M.; validation, L.M.M. and A.A.O.; formal analysis, L.M.M.; investigation, J.G. and L.M.M.; resources, J.G. and L.M.M.; data curation, L.M.M. and A.A.O.; writing—original draft preparation, L.M.M. and J.G.; writing—review and editing, L.M.M., R.J.G.II, A.A.O., S.Q.L., M.L.B., G.K.L., J.W.D. and J.G.; visualization, L.M.M.; supervision, J.G. and J.W.D.; project administration, J.G; funding acquisition, J.G. All authors have read and agreed to the published version of the manuscript.

Funding: This research was funded by the U.S. National Institute of Health-National Heart, Lung, and Blood Institute, grant numbers 1R15HL147299-01 and 1R01HL144739-01A1. Alexander Oliver is supported by the American heart Association grant #23PRE1012781.

Institutional Review Board Statement: The animal study protocol was approved by the Institutional Review Board of Michigan Technological University (protocol code 380482, 2021).

Informed Consent Statement: Not applicable.

Data Availability Statement: The authors are unable or have chosen not to specify which data have been used.

Conflicts of Interest: The authors declare no conflict of interest.

References

1. Iqbal, J.; Gunn, J.; Serruys, P.W. Coronary stents: Historical development, current status and future directions. *Br. Med Bull.* **2013**, *106*, 193–211. [CrossRef]
2. Hijazi, Z.M.; Homoud, M.; Aronovitz, M.J.; Smith, J.J.; Faller, G.T. A new platinum balloon-expandable stent (Angiostent) mounted on a high pressure balloon: Acute and late results in an atherogenic swine model. *J. Invasive Cardiol.* **1995**, *7*, 127–134. [PubMed]
3. Bhargava, B.; De Scheerder, I.; Ping, Q.B.; Yanming, H.; Chan, R.; Kim, H.S.; Kollum, M.; Cottin, Y.; Leon, M.B. A novel platinum-iridium, potentially gamma radioactive stent: Evaluation in a porcine model. *Catheter. Cardiovasc. Interv.* **2000**, *51*, 364–368. [CrossRef]
4. Oliver, A.A.; Ii, R.J.G.; Flom, K.L.; Morath, L.M.; Kolesar, T.M.; Mostaed, E.; Sikora-Jasinska, M.; Drelich, J.W.; Goldman, J. Analysis of Vascular Inflammation against Bioresorbable Zn–Ag-Based Alloys. *ACS Appl. Bio Mater.* **2020**, *3*, 6779–6789. [CrossRef]
5. Zhang, C.; Wen, T.H.; Razak, K.A.; Lin, J.; Xu, C.; Seo, C.; Villafana, E.; Jimenez, H.; Liu, H. Magnesium-based biodegradable microelectrodes for neural recording. *Mater. Sci. Eng. C* **2020**, *110*, 110614. [CrossRef]
6. Fineschi, M.; Gori, T. Very late thrombosis in a bare metal stent: An under-recognized problem. *Can. J. Cardiol.* **2008**, *24*, e6–e7. [CrossRef] [PubMed]
7. Zhang, S.H.; Reddick, R.L.; Piedrahita, J.A.; Maeda, N. Spontaneous Hypercholesterolemia and Arterial Lesions in Mice Lacking Apolipoprotein E. *Science* **1992**, *258*, 468–471. [CrossRef]
8. Getz, G.S.; Reardon, C.A. ApoE knockout and knockin mice: The history of their contribution to the understanding of atherogenesis. *J. Lipid Res.* **2016**, *57*, 758–766. [CrossRef] [PubMed]
9. Ali, Z.A.; Alp, N.J.; Lupton, H.; Arnold, N.; Bannister, T.; Hu, Y.; Mussa, S.; Wheatcroft, M.; Greaves, D.R.; Gunn, J.; et al. Increased In-Stent Stenosis in ApoE Knockout Mice. *Arter. Thromb. Vasc. Biol.* **2007**, *27*, 833–840. [CrossRef]
10. Matter, C.M.; Ma, L.; von Lukowicz, T.; Meier, P.; Lohmann, C.; Zhang, D.; Kilic, U.; Hofmann, E.; Ha, S.-W.; Hersberger, M.; et al. Increased Balloon-Induced Inflammation, Proliferation, and Neointima Formation in Apolipoprotein E (*ApoE*) Knockout Mice. *Stroke* **2006**, *37*, 2625–2632. [CrossRef]
11. Kim, M.; Sahu, A.; Hwang, Y.; Kim, G.B.; Nam, G.H.; Kim, I.-S.; Kwon, I.C.; Tae, G. Targeted delivery of anti-inflammatory cytokine by nanocarrier reduces atherosclerosis in ApoE$^{-/-}$ mice. *Biomaterials* **2019**, *226*, 119550. [CrossRef] [PubMed]
12. Liao, Z.-L.; Zeng, B.-H.; Wang, W.; Li, G.-H.; Wu, F.; Wang, L.; Zhong, Q.-P.; Wei, H.; Fang, X. Impact of the Consumption of Tea Polyphenols on Early Atherosclerotic Lesion Formation and Intestinal Bifidobacteria in High-Fat-Fed ApoE$^{-/-}$ Mice. *Front. Nutr.* **2016**, *3*, 42. [CrossRef] [PubMed]
13. Tung, M.-C.; Lan, Y.-W.; Li, H.-H.; Chen, H.-L.; Chen, S.-Y.; Chen, Y.-H.; Lin, C.-C.; Tu, M.-Y.; Chen, C.-M. Kefir peptides alleviate high-fat diet-induced atherosclerosis by attenuating macrophage accumulation and oxidative stress in ApoE knockout mice. *Sci. Rep.* **2020**, *10*, 8802. [CrossRef] [PubMed]
14. Pierson, D.; Edick, J.; Tauscher, A.; Pokorney, E.; Bowen, P.; Gelbaugh, J.; Stinson, J.; Getty, H.; Lee, C.H.; Drelich, J.; et al. A simplified in vivo approach for evaluating the bioabsorbable behavior of candidate stent materials. *J. Biomed. Mater. Res. Part B Appl. Biomater.* **2011**, *100B*, 58–67. [CrossRef]
15. Guillory, R.J., II; Oliver, A.A.; Davis, E.K.; Earley, E.J.; Drelich, J.W.; Goldman, J. Preclinical In Vivo Evaluation and Screening of Zinc-Based Degradable Metals for Endovascular Stents. *JOM* **2019**, *71*, 1436–1446. [CrossRef] [PubMed]
16. Zhao, S.; Seitz, J.-M.; Eifler, R.; Maier, H.J.; Guillory, R.J.; Earley, E.J.; Drelich, A.; Goldman, J.; Drelich, J.W. Zn-Li alloy after extrusion and drawing: Structural, mechanical characterization, and biodegradation in abdominal aorta of rat. *Mater. Sci. Eng. C* **2017**, *76*, 301–312. [CrossRef]
17. Fu, J.; Su, Y.; Qin, Y.-X.; Zheng, Y.; Wang, Y.; Zhu, D. Evolution of metallic cardiovascular stent materials: A comparative study among stainless steel, magnesium and zinc. *Biomaterials* **2019**, *230*, 119641. [CrossRef]
18. Baltzer, N. Platinum Group Metals (PGMs) for Permanent Implantable Electronic Devices. In *Precious Metals for Biomedical Applications*; Elsevier: Amsterdam, The Netherlands, 2014.
19. Cowley, A.; Woodward, B. A Healthy Future: Platinum in Medical Applications. *Platin. Met. Rev.* **2011**, *55*, 98–107. [CrossRef]
20. Grewe, P.H.; Deneke, T.; Machraoui, A.; Barmeyer, J.; Müller, K.M. Acute and Chronic Tissue Response to Coronary Stent Im-plantation: Pathologic Findings in Humans. *J. Am. Coll. Cardiol.* **1999**, *35*, 157–163. [CrossRef]

21. Oppi, S.; Lüscher, T.F.; Stein, S. Mouse Models for Atherosclerosis Research—Which Is My Line? *Front. Cardiovasc. Med.* **2019**, *6*, 46. [CrossRef]
22. Lee, Y.T.; Lin, H.Y.; Chan, Y.W.F.; Li, K.H.C.; To, O.T.L.; Yan, B.P.; Liu, T.; Li, G.; Wong, W.T.; Keung, W.; et al. Mouse models of atherosclerosis: A historical perspective and recent advances. *Lipids Health Dis.* **2017**, *16*, 12. [CrossRef] [PubMed]
23. Wolf, D.; Ley, K. Immunity and Inflammation in Atherosclerosis. *Circ. Res.* **2019**, *124*, 315–327. [CrossRef]
24. Chaabane, C.; Otsuka, F.; Virmani, R.; Bochaton-Piallat, M.-L. Biological responses in stented arteries. *Cardiovasc. Res.* **2013**, *99*, 353–363. [CrossRef] [PubMed]
25. Huebsch, N.; Mooney, D.J. Inspiration and application in the evolution of biomaterials. *Nature* **2009**, *462*, 426–432. [CrossRef]
26. Yokoyama, S.; Takano, M.; Yamamoto, M.; Inami, S.; Sakai, S.; Okamatsu, K.; Okuni, S.; Seimiya, K.; Murakami, D.; Ohba, T.; et al. Extended Follow-Up by Serial Angioscopic Observation for Bare-Metal Stents in Native Coronary Arteries: From healing response to atherosclerotic transformation of neointima. *Circ. Cardiovasc. Interv.* **2009**, *2*, 205–212. [CrossRef] [PubMed]

Disclaimer/Publisher's Note: The statements, opinions and data contained in all publications are solely those of the individual author(s) and contributor(s) and not of MDPI and/or the editor(s). MDPI and/or the editor(s) disclaim responsibility for any injury to people or property resulting from any ideas, methods, instructions or products referred to in the content.